Chirality-dependent absorption and third-order polarizability spectra in open single-wall carbon nanotubes

D.-S. Wu, W.-D. Cheng,* H. Zhang, X.-D. Li, Y.-Z. Lan, D.-G. Chen, Y.-J. Gong, and Y.-C. Zhang

Fujian Institute of Research on the Structure of Matter, the Graduate School of the Chinese Academy of Sciences, State Key Laboratory of Structural Chemistry, Fuzhou, Fujian 350002, People's Republic of China

(Received 24 April 2003; published 8 September 2003)

The optimized configurations and electronic structures have been obtained based on the density-functional theory for finite open single-walled carbon nanotubes of (4,4) and (5,5). The calculated results show that the bond lengths, bond angles, and charge distributions at the tube ends are significantly different from those at the tube wall. Then, the electronic absorption spectra of the two tubes are calculated by the time-dependent density-functional theory. The evidences show agreement between the theoretical and available experimental results. A strong and wide absorption band occurs for the case of light polarized parallel to the tube axis; a weak absorption and large transparent range appear as the case of light polarized perpendicular to the tube axis. Finally, the dynamic third-order optical polarizabilities in the three optical processes are obtained in terms of the sum-over-states method combined with the above-mentioned method. It is found that the anisotropy of the polarizabilities is larger for the (4,4) than (5,5) tube, and the tube with a larger axial length and smaller diameter has a larger third-order optical polarizabilities at nonresonant frequencies. The largest third-order polarizability is in the direction of both the polarized light and basic light along with the tube axis, and two photon excitation states make main contributions to the polarizabilities of the (4,4) and (5,5) tubes.

DOI: 10.1103/PhysRevB.68.1254XX PACS number(s): 61.48.+c, 42.65.An, 71.15.Mb

I. INTRODUCTION

Since its discovery in 1991, carbon nanotubes have been the focus of intense interest worldwide. This extensive attention to carbon nanotubes is due to their promise to exhibit unique physical properties. The properties could impact broad areas of science and technology, ranging from super strong composites to nanoelectronics.[1–3] The remarkable electronic properties of carbon nanotubes offer the greatest intellectual challenges and potential for novel applications. For example, it was first predicted that single-walled carbon nanotubes (SWNT's) could exhibit either metallic or semiconducting behavior depending only on diameter and helicity by the theoretical calculations.[4–6] This ability to display fundamentally distinct electronic properties without changing the local bonding, which was experimentally demonstrated through atomically resolved scanning tunneling microscopy (STM) measurements,[7,8] sets nanotubes apart from all other nanowire materials.[9,10] In recent years, ultrasmall radius single-wall carbon nanotubes (SWNT's) are successfully grown inside inert $AlPO_4$-5 zeolite channels, and the nanotubes arranged in the channels have a narrow diameter distribution about 4 Å.[11] The absorption spectra of these tubes are able to be investigated by experiment and theory because the possible nanotube chiralities are reduced to three: (3,3), (5,0), and (4,2).[12–14] Moreover, the nonlinear optical properties of carbon nanotubes have been of considerable interest, not only because the nonlinear spectrum gives information on their electronic structure, but also because the nonlinear materials can be applied to optical devices.[15–20] Nonlinear optical (NLO) materials with large third-order nonlinear susceptibilities at the optical transparent region are indispensable for all-optical switching, modulating, and computing devices. The nonlinear absorption materials with large third-order optical susceptibility are used for optical limiters and tunable filters that can suppress undesired radiation. The carbon nanotubes used in nonlinear optical devices have promising features at frequencies greater than infrared frequencies of the lattice vibration, and the main contributions to optical nonlinearities originate from the one-dimension motion of delocalized π electrons at a fixed lattice ion configuration. In view of this situation one can expect that the carbon nanotubes will have fast nonlinear optical responses and large nonresonant third-order optical susceptibilities.

In this study, we first report the optimized configurations of finite open SWCN's (4,4) and (5,5) based on the density-functional theory. Then, we calculate the spectra of electronic absorption by the time-dependent density-functional theory and discuss their anisotropy. Finally, we compute the dynamic third-order optical polarizabilities in terms of the sum-over-states method combined with the time-dependent density-functional theory and understand the electronic origins of third-order polarizabilities for the two tubes.

II. COMPUTATIONAL PROCEDURES

A. Optimizations of geometrical configurations based on the density-functional theory

Initial geometries of the finite open SWCN's (4,4) and (5,5) can be constructed by cut strips and rolled up from an infinite graphite sheet, respectively. The two tubes can be specified by their chiral vectors $\mathbf{C}_h = n\mathbf{a}_1 + m\mathbf{a}_2$, where $\mathbf{a}_1$ and $\mathbf{a}_2$ are graphite primitive lattice vectors with $|\mathbf{a}_1| = |\mathbf{a}_2| = a = (C\text{-}C)(3^{1/2})$ and $n = m = 4$, or 5, C-C = 1.42 Å. The tube diameter and chirality are uniquely characterized by[3,21,22] $d = a(n^2 + m^2 + nm)^{1/2}/\pi$ and $\cos\theta = (n + m/2)/(n^2$

$+m^2+nm)^{1/2}$, respectively. The geometrical optimizations of the finite open SWCN's (4,4) and (5,5) are carried out at the B3LYP/3-21G level using the DFT method[23] of the GAUSSIAN 98 program.[24] During the optimized processes, a convergent value of RMS (root-mean-square) density matrix and the critical values of force and displacement are set by default of the GAUSSIAN 98 program. The obtained values that are less than these criterion are omitted during the calculations. Accordingly, after the convergences of the maximum force, RMS force, maximum displacement, and RMS displacement are reached, the zero of the first derivatives and the positive of the second derivatives are obtained on a potential-energy surface for these SWCN's. Zero length of the all gradient vectors (first derivatives) characterizes a stationary point, and a minimum corresponds to a point having positive second derivatives. Equivalently, all forces on the atoms in a finite open SWCN are zero, and the force constant is positive. In classical mechanics, the first derivative of the potential energy for a particle is minus the force on the particle, and the second derivative is the force constant. Hence a stationary point of minimum on energy surfaces corresponds to equilibrium geometry of these SWCN's.

B. Calculations of absorption spectra based on time-dependent density-functional theory

After the optimized geometries of the finite open SWCN's (4,4) and (5,5) are obtained, we employ the time-dependent density-functional theory[25–27] at the B3LYP/3-21G level (TDB3LYP/3-21G) and run in the program of GAUSSIAN 98 in the calculations of the transition moments and excited-state energies of these configurations. Here, the B3LYP designs the Becke exchange function combined with three parameter of Lee-Yang-Parr hybrid correlation function, which includes both local and nonlocal terms.[23,28,29] The ground state and all excited states were multiplicities of one. In the TDB3LYP calculations the core electrons were frozen and inner shells were excluded from the correlation calculations. The range of molecular orbitals for correlation is from orbital 65 to orbital 576, orbital 81 to orbital 720, individually for the SWCN's (4,4) and (5,5) in the all calculations. The wave functions and energy eigenvalues of the excited states were determined by solving the time-dependent Kohn-Sham equation.[26] The SCF convergence criterion of the RMS density matrix and the maximum density matrix is set at 10^{-8} and 10^{-6}, respectively, in the excited-state calculations. The iterations of excited states are continued until the changes on energies of states are no more than 10^{-7} a.u. between the iterations, and the convergence has been obtained in the all calculations of excited states.

C. Calculations of third-order polarizabilities based on sum-over-states method

The tensor components of the frequency-dependent and nonresonant third-order polarizability γ of finite open SWCN's are calculated by the conventional sum-over-states (SOS) method:[30,31]

$$\begin{aligned}\gamma_{abcd}(-\omega_p;\omega_1,\omega_2,\omega_3) &= (2\pi/h)^3 K(-\omega_p;\omega_1,\omega_2,\omega_3)e^4 \\ &\times\Bigg(\sum\nolimits_P\Bigg\{\sum\nolimits'_{i,j,k}(\langle o|r_a|k\rangle\langle k|r_b^*|j\rangle\langle j|r_c^*|i\rangle \\ &\times\langle i|r_d|o\rangle)/[(\omega_{ko}-\omega_p)(\omega_{jo}-\omega_1-\omega_2) \\ &\times(\omega_{io}-\omega_1)]\Bigg\}-\sum\nolimits_P\Bigg\{\sum\nolimits'_{j,k}(\langle o|r_a|j\rangle\langle j|r_b|o\rangle \\ &\times\langle o|r_c|k\rangle\langle k|r_d|o\rangle)/[(\omega_{jo}-\omega_p)(\omega_{jo}-\omega_1) \\ &\times(\omega_{ko}+\omega_2)]\Bigg\}\Bigg). \qquad (1)\end{aligned}$$

Hereafter the mark $\gamma(3\omega)$, $\gamma(2\omega)$, and $\gamma(\omega)$ symbolizes the third-order polarizability of third-harmonic generation (THG) of $\gamma(-3\omega;\omega,\omega,\omega)$, electric-field-induced second-harmonic generation (EFISHG) of $\gamma(-2\omega;\omega,\omega,0)$ and degenerate four-wave mixing (DFWM) of $\gamma(-\omega;\omega,\omega,-\omega)$, individually. The prefactor $K(-\omega_p;\omega_1,\omega_2,\omega_3)$ must be taken as the same value for the THG, EFISHG, and DFWM at the static case of an input photon energy of zero, and it is the relative magnitudes of the reference state (ground state) nonlinear polarizabilities for each optical process at nonzero frequency (detailed descriptions in the Appendix).[31] In the following calculations, we use the same prefactor K in order

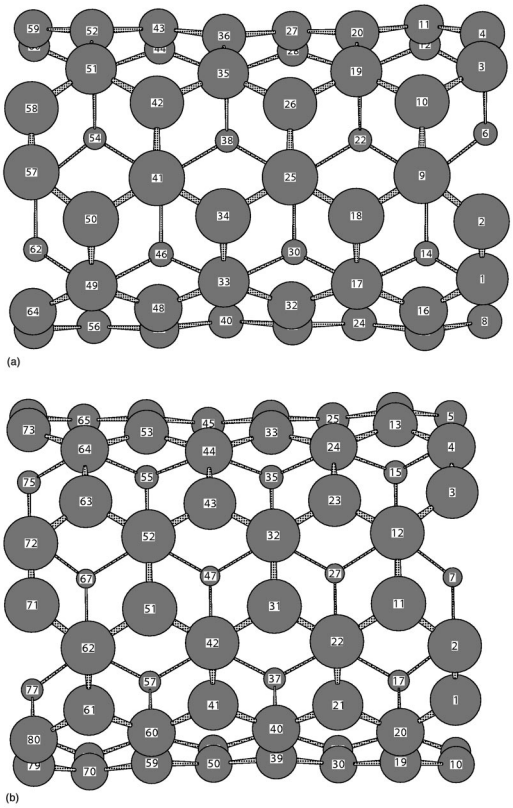

FIG. 1. (a) The optimized geometrical structures of finite open SWCN's (4,4). (b) The optimized geometrical structures of finite open SWCN's (5,5).

TABLE I. Some selected bond lengths and angles of SWCN (4,4) and SWCN (5,5).

SWCN (4,4)				SWCN (5,5)			
Bond lengths		Bond angle		Bond lengths		Bond angle	
C(1)-C(2)	1.237	C(2)-C(1)-C(16)	126.230	C(1)-C(2)	1.236	C(2)-C(1)-C(20)	126.859
C(1)-C(16)	1.414	C(1)-C(2)-C(9)	126.266	C(1)-C(20)	1.413	C(1)-C(2)-C(11)	126.873
C(2)-C(9)	1.414	C(4)-C(3)-C(10)	126.232	C(2)-C(11)	1.413	C(4)-C(3)-C(12)	126.854
C(3)-C(4)	1.237	C(3)-C(4)-C(11)	126.263	C(3)-C(4)	1.236	C(3)-C(4)-C(13)	126.882
C(3)-C(10)	1.414	C(6)-C(5)-C(12)	126.235	C(5)-C(6)	1.237	C(8)-C(7)-C(16)	126.861
C(6)-C(13)	1.414	C(2)-C(9)-C(10)	123.749	C(5)-C(14)	1.413	C(7)-C(8)-C(17)	126.849
C(7)-C(8)	1.237	C(2)-C(9)-C(18)	109.680	C(7)-C(8)	1.237	C(9)-C(10)-C(19)	126.845
C(9)-C(10)	1.426	C(3)-C(10)-C(19)	109.689	C(8)-C(17)	1.413	C(2)-C(11)-C(22)	109.830
C(9)-C(18)	1.451	C(9)-C(10)-C(19)	118.195	C(11)-C(12)	1.417	C(11)-C(12)-C(23)	118.987
C(17)-C(18)	1.460	C(7)-C(14)-C(23)	109.690	C(11)-C(22)	1.452	C(4)-C(13)-C(14)	125.821
C(18)-C(25)	1.431	C(8)-C(15)-C(16)	123.747	C(14)-C(25)	1.452	C(5)-C(14)-C(25)	109.837

to make the remark to justify plotting curves for the three types of nonlinear polarizability against common axes.

III. RESULTS AND DISCUSSIONS

A. Geometries and electronic structures at ground state

Figure 1 shows the optimized geometrical structures of finite open SWCN's (4,4) and (5,5). It is found that their configurations are armchair, and that the (4,4) and (5,5) tube is separately consisted of 64 and 80 carbon atoms. For the (4,4) tube, the tube axial length and diameter of the optimized geometry are about 8.451 and 5.615 Å, the range of C-C length is from 1.414 to 1.460 Å and falls well between single (1.54 Å) and double (1.34 Å) bonds of C-C except the C-C bonds of tube ends. There are four pairs of C-C bonds being 1.237 Å at each end of open tube, and the C-C lengths have triplet bond character (1.20 Å). The range of C-C-C bond angle is from 110º to 126º, and the tube (4,4) appears as curvature where requires the C atom to be pyramidalized. For the (5,5) tube, the axial length and diameter are about 8.449 and 6.971 Å, the C-C bonds in the nanotube wall are more average (ranging from 1.413 to 1.452 Å), and there are separately five pairs of C-C bonds in the two ends being the same lengths as those of the two ends of (4,4) tube. Table I lists the selected bond lengths and angles for the finite SWCN's (4,4) and (5,5). The bond lengths and angles of the relaxed structures, especially at the tube ends, are substantially different from those of an ideal rolling of a graphene sheet.

The calculated electronic populations at ground state show that there are four types of charge distributions in the SWCN's, as listed in Table II. The atoms localized in SWCN ends donate more electrons and have larger positive charges. The atoms directly connected with end atoms accept electrons and have negative charges. The other two typical charge distributions show that the atoms more towards the middle wall of tube are more close to electronic neutral. The calculated gap energy corresponding to the difference of the HOMO (highest occupied molecular orbital) and LUMO (lowest unoccupied molecular orbital) eigenvalues of the TDB3LYP ground state is 1.79 and 1.61 eV for the (4,4) and (5,5) tubes, respectively. The results indicate that the smaller the diameter the larger the HOMO-LUMO gap in open SWCN's. M. Machon and H. J. Liu groups separately reported the gap between the valence and conduction bands at the Γ point of the (3,3) tube to be about 2.6 eV (Fig. 3 and Fig. 2 in Ref. 13 and 14, respectively), which is obtained from the energy band calculations based on the local-density approximation density-functional theory (LDA-DFT) method.[13,14] In spite of the obtained values based on the different method from ours, we also find a variation trend that there is a larger gap in a smaller diameter of SWCN's, comparing them with our obtained results of (4,4) and (5,5) tubes.

TABLE II. Charge distributions (e) of SWCN.

Types	C-end	C-second	C-third	C-fourth
(4,4)	0.059	−0.082	0.021	0.001
(5,5)	0.061	−0.081	0.020	0.000

B. Electronic absorption spectrum of ground state

The calculated electronic absorption spectra of the finite open SWCN's (4,4) and (5,5) are shown in Fig. 2. Comparing the absorption spectra between the two tubes, we find that the spectrum of the (4,4) tube with the axial length of 8.451 Å and diameter of 5.615 Å gives a sharp absorption peak and makes a blue shift. Our calculations also predict a variety of the spectral shapes and peak positions of the two tubes. It is found from Fig. 2 that the spectra of these tubes exhibit long absorption tails, which extend deep into the region of the lower transition energies. The first absorption peak of S_a is localized at about 550 and 570 nm, and the second peak of S_r is localized at about 400 and 437 nm for the finite (4,4) and (5,5) tubes, respectively. From the transition moments in the axial (z) and radial (x,y) directions listed in Table III, we can find that the absorption of S_a is mostly originated from an axial allowed electron transition from the ground state to excited state 12 for the (4,4) tube and to excited state 10 for the (5,5) tube, and the absorption of S_r is mostly originated from a radical allowed electron

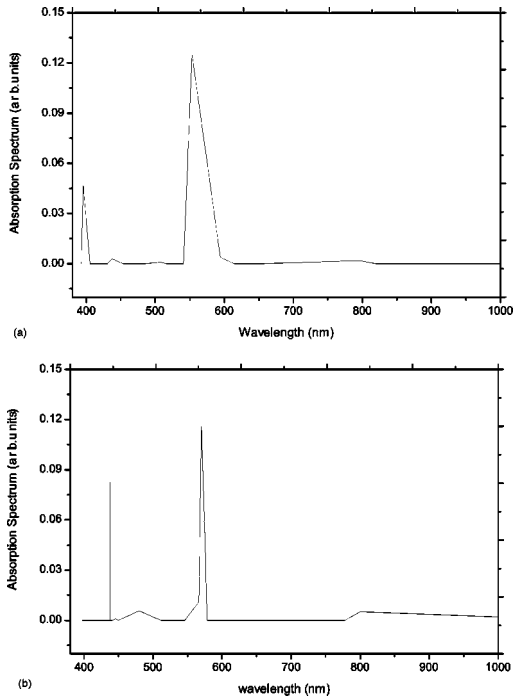

FIG. 2. (a) The calculated absorption spectrum of SWCN (4,4) based on TDB3LYP/3-21 level. (b) The calculated absorption spectrum of SWCN (5,5) based on TDB3LYP/3-21 level.

transition from the ground state to excited state 35 for the (4,4) tube and to excited state 27 for the (5,5) tube, respectively. An analysis in terms of the results calculated by the TDB3LYP method shows that the absorption peaks of the largest wavelength (S_a) are mainly contributions from the charge transfers from π bonding to π^* antibonding orbitals. For example, the excited state S_{12} is mostly constructed by the configurations of $0.4150(\mathrm{MO}_{191}\rightarrow\mathrm{MO}_{193})$ $+0.3218(\mathrm{MO}_{192}\rightarrow\mathrm{MO}_{196})$, and S_{10} is mostly constructed by the configuration of $0.4697(\mathrm{MO}_{239}\rightarrow\mathrm{MO}_{241})$ $+0.2907(\mathrm{MO}_{240}\rightarrow\mathrm{MO}_{242})$ for the finite open SWCN's (4,4) and (5,5), respectively. The compositions of the molecular orbitals contributing to these configurations are mostly originated from the p_π orbitals of the SWCN's. Figure 3 give the plots of the HOMO (highest occupied molecular orbital is separately orbital 192 and 240) and LUMO (lowest unoccupied molecular orbital is separately orbital 193 and 242) of the SWCN's (4,4) and (5,5), respectively. They describe the pictures of $\pi-\pi$ interactions. In view of the configuration structures and orbital positions, the absorptions of S_r are also assigned as the electron transition between the $\sigma-\pi$ hybridized orbitals.

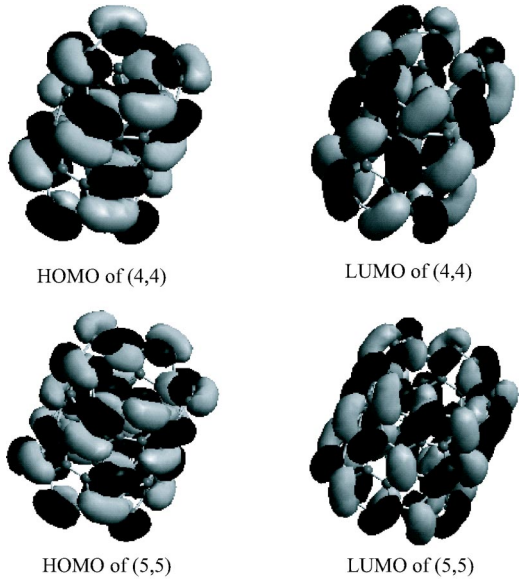

FIG. 3. The HOMO and LUMO of finite open SWCN's (4,4) and (5,5).

We noted in the reports of polarized absorption spectra 4-Å diameter single-walled carbon nanotubes.[11–14] It is difficult to make direct comparisons between our results and reported ones due to different diameter and length in the SWCN's. However, the two evidences are in agreement. A strong and broad absorption band occurs at a lower energy region for the case of light polarized parallel to the tube axis. Our calculated oscillator strength in this direction is 0.025 and 0.023, and the transition energy is 2.24 and 2.17 eV, which correspond to strong absorption for the (4,4) and (5,5) tubes, respectively. Here, the calculated transition energy is defined as a difference between the energies of the excited and ground states based on the TDB3LYP/3-21 level. Our calculated energies fall between the sharp peaks at 2.8 eV for tube (3,3) and 1.9 eV for tube (4,2) calculated by Liu and Chan.[13] The other evidence is that a weak absorption and large transparent range appear in the infrared and visible lights for the case of light polarized perpendicular to the tube axis. Our calculated oscillator strength in the radial direction is 0.009 and 0.017, and the transition energy is 3.13 and 2.84 eV for the (4,4) and (5,5) tubes, respectively. The calculated cutoff edge of transparency is less about 1.0 eV than that of the measurement of 4-Å diameter single-walled carbon nanotubes.[11]

C. Third-order nonlinear optical properties of ground state

Before attempting to compute the variation of the third-order polarizability vs wavelength, it is necessary to investi-

TABLE III. The selected transition moments and energies of (4,4) and (5,5) tubes.

	(4,4)				(5,5)			
Band	Moment (a.u.)			Energy (eV)	Moment (a.u.)			Energy (eV)
	x	y	z		x	y	z	
S_a	0.000	0.000	−2.355	2.2418	−0.000	−0.008	2.336	2.1738
S_r	−1.007	−0.212	0.000	3.1318	−1.264	−0.821	0.000	2.8364

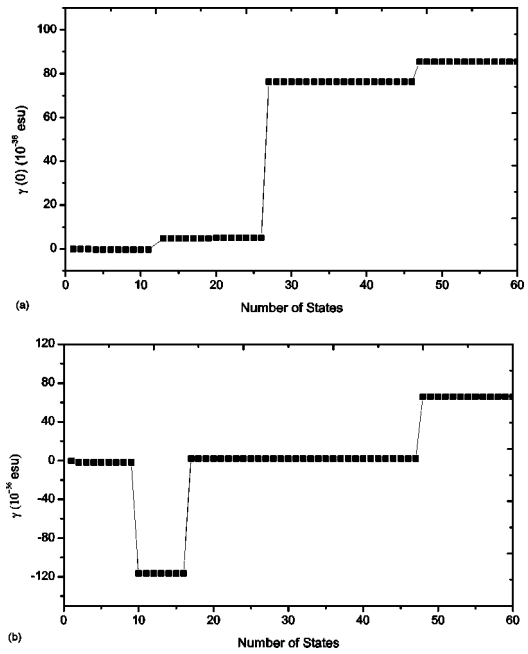

FIG. 4. (a) Convergent behavior of third-order polarizabilities of finite open SWCN (4,4). (b) Convergent behavior of third-order polarizabilities of finite open SWCN (5,5).

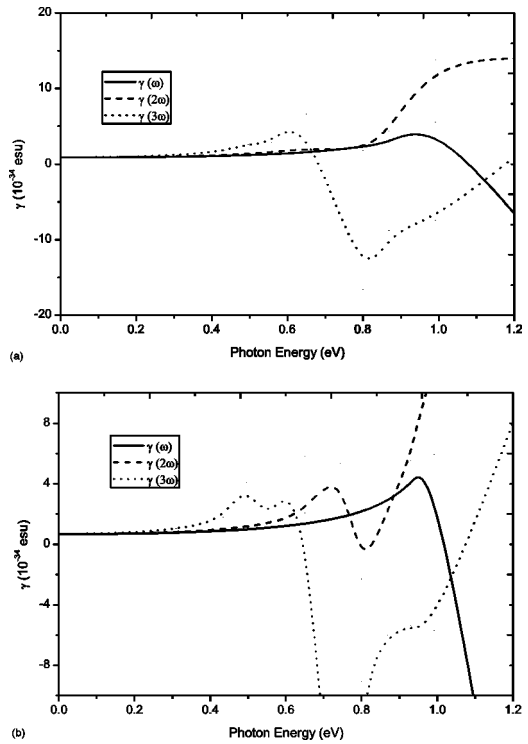

FIG. 5. (a) Dynamic behavior of third-order polarizabilities of SWCN (4,4) based on SOS//TDB3LYP/3-21 G level. (b) Dynamic behavior of third-order polarizabilities of finite open SWCN (5,5) based on SOS//TDB3LP/3-21 G level.

gate the behavior of the convergence in the summation of excited states and to determine whether the results calculated from the TDB3LYP method are reliable for the finite open SWCN's (4,4) and (5,5). Figure 4 show the plots of the calculated third-order polarizabilities $\gamma_a(\gamma_{zzzz})$ for which the polarizability is along with the axial direction of tubes vs the number of states of the tubes (4,4) and (5,5) at the static case. It is found that the calculated value of γ_a including 48 states is about 100% of the γ_a value including 60 states, and the 27th state of the (4,4) tube and 48th state of the (5,5) tube separately makes significant contributions to the third-order polarizabilities of γ_a. This shows a reasonable approximation truncating the infinite SOS expansion to a finite one over about 60 states in our calculations of γ.

Figure 5 depicts the calculated dynamic third-order polarizabilities of γ_a having different optical physical processes from frequency 0.0 to 1.20 eV/$\hbar$ at the ground state. For the static case where the input photon energy is zero, the γ_a values of all three processes of THG, EFISHG, and DFWM have the same values of 0.86×10^{-34}, and 0.66×10^{-34} esu for the finite open SWCN's (4,4) and (5,5), respectively. These values are close to the calculated values at ground state of C_{60} and C_{70} in magnitude order.[32] Furthermore, at the dynamic case when an input energy of $h\omega$ is 0.80 eV (1550 nm), $\gamma_a(\omega)$, $\gamma_a(2\omega)$, and $\gamma_a(3\omega)$ are individually 2.23×10^{-34}, 1.81×10^{-34}, and -16.62×10^{-34} esu for the (4,4) tube; 2.13×10^{-34}, -2.23×10^{-34}, and -9.07×10^{-34} esu for the (5,5) tube, respectively. In order to describe the anisotropy of nonlinear polarizabilities of the tubes (4,4) and (5,5), Table IV lists the calculated third-order polarizabilities at the radial and axial directions of the tubes in the static case. It is shown that the largest third-order polarizability is in the direction of the polarized and basic light along with the tube axis. Comparing the third-order polarizabilities of the (4,4) tube and those of the (5,5) tube, we found that the anisotropy of polarizabilities is larger for the (4,4) than (5,5) tube, and there is a larger third-order polarizability in the axial direction while there is a smaller diameter in the finite open SWCN's.

Now, we are going to discuss the electronic origin of third-order polarizabilities of the SWCN's (4,4) and (5,5). In the SOS formula of Eq. (1), we can see the value of third-order polarizability comes from the summations of type-I and type-II terms. These two terms are the competing third-order virtual excitation processes, and the electron transitions between two states in each term are fit for the dipole selection rules. The type-I processes are of the form $S_g\rightarrow S_m\rightarrow S_g\rightarrow S_m\rightarrow S_g$, where S_g is the ground state and S_m is a one-photon allowed excited state. The intermediate state is S_g itself, and this process makes a negative contribution to γ at a low-frequency region. For example, the calculated $[\gamma_a(0)]_I$ is -0.941×10^{-34}, and -1.163×10^{-34} esu at

TABLE IV. The calculated static polarizabilities of γ (10^{-36} esu).

Tube	γ_{xxxx}	γ_{yyyy}	γ_{zzzz}	$\langle\gamma\rangle^a$
(4,4)	5.85	5.85	85.59	30.67
(5,5)	9.89	9.76	65.79	49.37

[a] $\langle\gamma\rangle=1/5(\gamma_{xxxx}+\gamma_{yyyy}+\gamma_{zzzz}+\gamma_{xxyy}+\gamma_{xxzz}+\gamma_{yyxx}+\gamma_{yyzz}+\gamma_{zzxx}+\gamma_{zzyy})$.

static case, and the calculated dynamic $[\gamma_a(\omega)]_I$, $[\gamma_a(2\omega)]_I$, and $[\gamma_a(3\omega)]_I$ is -1.287×10^{-34}, -1.705×10^{-34}, and -3.863×10^{-34} esu for the (4,4) tube; -1.665×10^{-34}, -2.390×10^{-34}, and -5.402×10^{-34} esu for the (5,5) tube, respectively, at an input photon energy of 0.650 eV. For the type-II processes, $S_g\rightarrow S_m\rightarrow S_n\rightarrow S_m\rightarrow S_g$, the intermediate state S_n is a two-photon allowed excited state. The obtained results illustrate the electron density redistribution for the virtual transitions $S_g\rightarrow S_m$ and $S_m\rightarrow S_n$, which are important to the type-I and type-II terms, respectively. From an analysis of the summation over states of type-I and type-II terms, respectively, we can find that the 12th excited state is the important one-photon state contributing to third-order polarizabilities and the 27th excited state is the important two-photon state contributing to third-order polarizabilities in the axial direction of the (4,4) tube. The transition of from S_g to S_{12}, and to S_{27} separately yields a transition moment of -5.9862 and -0.0013 debye, in contrast, the transition $S_{27}\rightarrow S_{12}$ produces a large transition moment of -7.2005 Debye in axial direction, which dominates the positive type-II contributing term in $\gamma_a(0)$. The type-II process makes a larger, positive contribution to γ_a and therefore determines the overall sign of γ_a to be positive, a result that is corroborated by theoretical values. For instances, the calculated $[\gamma_a(0)]_{II}$ is 1.796×10^{-34}, and 1.821×10^{-34} esu for the tubes (4,4) and (5,5) at static case, and the calculated $[\gamma_a(\omega)]_{II}$, $[\gamma_a(2\omega)]_{II}$, $[\gamma_a(3\omega)]_{II}$ is 2.799×10^{-34}, 3.724×10^{-34}, and 10.496×10^{-34} esu; 2.996×10^{-34}, 4.462×10^{-34}, and 11.208×10^{-34} esu at an input photon energy of 0.650 eV for the tubes (4,4) and (5,5), respectively. From the above analysis, we can infer a large value of γ_a from a large value of $(\gamma_a)_{II}$, that is, the two-photon excitation processes greatly win a triumph over the one-photon excitation processes.

We note that the experimental values of $\chi^{(3)}$ is 6.460×10^{-14} esu at fundamental wavelength 1064 nm measured with the 30-ps-wide pulse laser for the carbon nanotube,[19] and is 4×10^{-13} esu at wavelength 820 nm for the SWCN of diameter 1.3 nm and length 160 nm.[17] The calculated values of $\chi^{(3)}$ ($1.3–1.5\times10^{-13}$ esu) at input wavelength of 1907 nm is in agreement with the experimental $\chi^{(3)}$ value of the SWCN in the order of magnitude, considering the molecular density number of SWCN's (4,4) and (5,5) in the magnitude order of 10^{21} while we omit the interactions between the nanotubes and use the relation of $\chi^{(3)}=N\gamma=\gamma/V$. Here, N is the nanotube density number and V is the nanotube volume.

IV. CONCLUSIONS

The geometrical structures of finite open SWCN's (4,4) and (5,5) have been optimized based on B3LYP/3-21 G level. The optimized structures show that the bond lengths and angles of the tubes, in particular, at the tube ends, are substantial differences from those of an ideal rolling of a graphene sheet. The electronic absorption spectra have been calculated based on the TDB3LYP/3-21 G level, and the dynamic third-order optical polarizabilities in the THG, EFISHG, and DFWM optical processes have been obtained by the SOS combined with the TDB3LYP methods for the optimized configurations of the (4,4) and (5,5) tubes. The first absorption band is mostly originated from an axial allowed electron transition between π and π^* orbitals, and the second absorption band is mostly originated from a radical allowed electron transition between the $\sigma-\pi$ hybridized orbitals. The calculated results are in agreement with the experimental evidences,[13] that is, a strong absorption and small transparent range occurs for the case of light polarized parallel to the tube axis; a weak absorption and large transparent range appear as the case of light polarized perpendicular to the tube axis. The calculated results show that the largest third-order polarizability is in the direction of the polarized and basic light along with the tube axis, and these polarizabilities are originated from the two photon allowed excitation states. The anisotropy of third-order polarizabilities is larger for the (4,4) than (5,5) tube, and there is a larger third-order polarizability at the axial direction in a smaller diameter of the SWCN.

APPENDIX

The expression of third-order polarizibility is obtained by application of time-dependent perturbation theory to the interacting electromagnetic field and microscopic system. Straightforward application of standard quantum-mechanical time-dependent perturbation theory, however, leads to unphysical secular divergences in $\gamma_{abcd}(-\omega_p;\omega_1,\omega_2,\omega_3)$ when any subset of the frequencies ω_1, ω_2, and ω_3 sums to zero. The secular divergences, which results from the failure of the standard perturbation theory to properly consider the slowly varying components of the perturbed wave function, are eliminated by employed damping factor $i\Gamma$, as described in the following:

$$\begin{aligned}\gamma_{abcd}(-\omega_p;\omega_1,\omega_2,\omega_3)&=(2\pi/h)^3K(-\omega_p;\omega_1,\omega_2,\omega_3)e^4\\&\times\Bigg(\sum{}_P\Bigg\{\sum{}'_{i,j,k}(\langle o|r_a|k\rangle\langle k|r_b^*|j\rangle\langle j|r_c^*|i\rangle\\&\times\langle i|r_d|o\rangle)/[(\omega_{ko}-\omega_p-i\Gamma_{ko})(\omega_{jo}-\omega_1-\omega_2-i\Gamma_{jo})\\&\times(\omega_{io}-\omega_1-i\Gamma_{io})]\Bigg\}-\sum{}_P\Bigg\{\sum{}'_{j,k}(\langle o|r_a|j\rangle\\&\times\langle j|r_b|o\rangle\langle o|r_c|k\rangle\langle k|r_d|o\rangle)/[(\omega_{jo}-\omega_p-i\Gamma_{jo})\\&\times(\omega_{jo}-\omega_1-i\Gamma_{jo})(\omega_{ko}+\omega_2+i\Gamma_{ko})]\Bigg\}\Bigg).\end{aligned}\tag{2}$$

Here, the $\langle o|r_a|k\rangle$ is a electronic transition moment along the a axis of a Cartesian system, between the reference state $<o$ and excited state $\langle k$; the $\langle k|r_b^*|j\rangle$ denotes the dipole difference operator equal to $[\langle k|r_b|j\rangle-\langle o|r_b|o\rangle\delta_{kj}]$; the $\hbar\omega_{ko}$ is the energy difference between state k and reference state o. The $\hbar\omega_{ko}$, transition moments and dipole moments can be obtained from the calculated results based on the TDB3LYP or other quantum chemical method. The ω_1, ω_2, and ω_3 are the frequencies of the perturbating radiation fields; the $\omega_p=\omega_1+\omega_2+\omega_3$ is the polarization response fre-

quency. The Σ_P indicates an average over all permutations of ω_p, ω_1, ω_2, and ω_3 along with associated indices *a*, *b*, *c*, and *d*; the Σ' indicates a sum over all states but reference state *o*. The factor $K(-\omega_p;\omega_1,\omega_2,\omega_3)$ accounts for distinguishable permutations of the input frequencies and cases arising from the definition of the electric-field amplitudes.[30] The value of $K(-\omega_p;\omega_1,\omega_2,\omega_3)$ is given by $2^{-m}D$ where *m* is the number of nonzero input frequencies minus the number of nonzero output frequencies and *D* is the number of distinguishable orderings of the set $\omega_1,\omega_2,\omega_3$. As specific examples, for third harmonic generation (THG), $K(-3\omega;\omega,\omega,\omega)=1/4$, and for degenerate four-wave mixing (DFWM), $K(-\omega;\omega,\omega,-\omega)=3/4$. Accordingly, when input and output frequencies are all zero, i.e., the static case, $K(0;0,0,0)=1$ for the THG, EFISHG, and DFWM optical processes. In practical calculations, if ω_1, ω_2, and ω_3 (as well as their arbitrary linear combinations) can be chosen to be away from a resonant frequency, all the damping factors $i\Gamma$ can be neglected, and formula (2) will be reduced as formula (1). In this way, although the damping factors are not included in this equation, the resonant divergences will be able to be avoided in the calculations.

ACKNOWLEDGMENTS

We are grateful to the National Science Foundation of China (Grant No. 90201015), the Science Foundation of the Fujian Province (Grant Nos. E0210028 and 2002F010), and the Foundation of State Key Laboratory of Structural Chemistry (Grant No. 030060) for financial support.

*Corresponding author. Email address: cwd@ms.fjirsm.ac.cn

[1] M. S. Dresselhaus, G. Dresselhaus, and P. C. Eklund, *Science of Fullerenes and Carbon Nanotubes* (Academic, San Diego, 1996).
[2] B.I. Yakobson and R.E. Smalley, Am. Sci. **85**, 324 (1997).
[3] C. Dekker, Phys. Today **52** (5), 22 (1999).
[4] N. Hamada, S. Sawada, and A. Oshiyama, Phys. Rev. Lett. **68**, 1579 (1992).
[5] J.W. Mintmire, B.I. Dunlap, and C.T. White, Phys. Rev. Lett. **68**, 631 (1992).
[6] R. Saito, M. Fujita, G. Dresselhaus, and M.S. Dresselhaus, Appl. Phys. Lett. **60**, 2204 (1992).
[7] J.W.G. Wildoer, L.C. Venema, A.G. Rinzler, R.E. Smalley, and C. Dekker, Nature (London) **391**, 59 (1998).
[8] T.W. Odom, J.-L. Huang, P. Kim, and C.M. Lieber, Nature (London) **391**, 62 (1998).
[9] C.M. Lieber, Solid State Commun. **107**, 607 (1998).
[10] J. Hu, T.W. Odom, and C.M. Lieber, Acc. Chem. Res. **32**, 435 (1999).
[11] Z.M. Li, Z.K. Tang, H.J. Liu, N. Wang, C.T. Chan, R. Saito, S. Okada, G.D. Li, J.S. Chen, N. Nagasawa, and S. Tsuda, Phys. Rev. Lett. **87**, 127401 (2001).
[12] W.Z. Liang, G.H. Chen, Z.M. Li, and Z.-K. Tang, Appl. Phys. Lett. **80**, 3415 (2002).
[13] H.J. Liu and C.T. Chan, Phys. Rev. B **66**, 115416 (2002).
[14] M. Machon, S. Reich, C. Thomsen, D. Sanchez-Portal, and P. Ordejon, Phys. Rev. B **66**, 155410 (2002).
[15] C. Stanciu, R. Ehlich, V. Petrov, O. Steinkellner, J. Herrmann, I. V. Hertel, G.Y. Slepyan, A.A. Khrutchinski, S.A. Maksimenko, F. Rotermund, E.E.B. Campbell, and F. Rohmund, Appl. Phys. Lett. **81**, 4064 (2002).
[16] L. Vivien, P. Lancon, D. Riehl, F. Hache, and E. Anglaret, Carbon **40**, 1789 (2002).
[17] S. Wang, W. Huang, H. Yang, Q. Gong, Z. Shi, X. Zhou, D. Qiang, and Z. Gu, Chem. Phys. Lett. **320**, 411 (2000).
[18] VI.A. Margulis, E.A. Gaiduk, and E.N. Zhidkin, Diamond Relat. Mater. **8**, 1240 (1999).
[19] X. Liu, J. Si, B. Chang, G. Xu, Q. Yang, Z. Pan, S. Xie, and P. Ye, Appl. Phys. Lett. **74**, 164 (1999).
[20] VI.A. Margulis and T.A. Sizikova, Physica B **245**, 173 (1998).
[21] J.W. Ding, X.H. Yan, and J.X. Cao, Phys. Rev. B **66**, 073401 (2002).
[22] M.S. Dresselhaus, Nature (London) **391**, 19 (1998); Science **292**, 560 (2001).
[23] A.D. Becke, J. Chem. Phys. **98**, 5648 (1993).
[24] GAUSSIAN 98 (Revision A.9), M. J. Frisch, G. W. Trucks, H. B. Schlegel, G. E. Scuseria, M. A. Robb, J. R. Cheeseman, V. G. Zakrzewski, J. A. Montgomery, R. E. Stratmann, J. C. Burant, S. Dapprich, J. M. Millam, A. D. Daniels, K. N. Kudin, M. C. Strain, O. Farkas, J. Tomasi, V. Barone, M. Cossi, R. Cammi, B. Mennucci, C. Pomelli, C. Adamo, S. Clifford, J. Ochterski, G. A. Petersson, P. Y. Ayala, Q. Cui, K. Morokuma, D. K. Malick, A. D. Rabuck, K. Raghavachari, J. B. Foresman, J. Cioslowski, J. V. Ortiz, B. B. Stefanov, G. Liu, A. Liashenko, P. Piskorz, I. Komaromi, R. Gomperts, R. L. Martin, D. J. Fox, T. Keith, M. A. Al-Laham, C. Y. Peng, A. Nanayakkara, C. Gonzalez, M. Challacombe, P. M. W. Gill, B. G. Johnson, W. Chen, M. W. Wong, J. L. Andres, M. Head-Gordon, E. S. Replogle, and J. A. Pople, Gaussian, Inc., Pittsburgh PA, 1998.
[25] M.E. Casida, C. Jamorski, K.C. Casida, and D.R. Salahub, J. Chem. Phys. **180**, 4439 (1988).
[26] R. Bauernschmitt and R. Ahlrichs, Chem. Phys. Lett. **256**, 454 (1996).
[27] R.E. Stratman, G.E. Scuseria, and M.J. Frisch, J. Chem. Phys. **109**, 8218 (1998).
[28] C. Lee, W. Yang, and R.G. Parr, Phys. Rev. B **37**, 785 (1988).
[29] B. Miehlich, A. Savin, H. Stoll, and H. Preuss, Chem. Phys. Lett. **157**, 2000 (1989).
[30] B.J. Orr and J.F. Ward, Mol. Phys. **20**, 513 (1971).
[31] B.M. Pierce, J. Chem. Phys. **91**, 791 (1989).
[32] W.-D. Cheng, D.-S. Wu, H. Zhang, D.-G. Chen, and H.-X. Wang, Phys. Rev. B **66**, 113401 (2002).